ANNALS OF GEOPHYSICS, 62, 5, SE559, 2019; doi: 10.4401/ag-7922

"ESTIMATION OF SOURCE AND SITE CHARACTERISTICS IN THE NORTH-WEST HIMALAYA USING THE GENERALIZED INVERSION METHOD"

Nelliparambil Hareeshkumar Harinarayan[1], Abhishek Kumar[*,1]

(1) Department of Civil Engineering, Indian Institute of Technology Guwahati, Assam, India

Article history

Receveid **September 13, 2018**; accepted **March 5, 2019**.

Subject classification:

Magnetospheric scaling relation, source characteristics, stress drop, apparent stress, site characteristics, Generalized Inversion, HVSR.

ABSTRACT

A site constraint generalized inversion technique (GINV) has been used in the present study to develop source and site spectra for the regions in and around north–west Himalaya. Database consists of 156 earthquake (EQ) records corresponding to 21 EQ events [2.5<magnitude (M)<5.8], recorded at 78 recording stations. Source parameters like scalar moment(M_0), corner frequency(f_c), stress drop($\Delta\sigma$), apparent stress drop(σ_A), and seismic energy(E_S) are computed for each EQ event by fitting the point source model to the obtained source spectra. Calculated M_0 and f_c values for all events are found in the range of 4.96×10^{13}Nm–2.91×10^{16}Nm and 1.50Hz–5.50Hz respectively. Further, regression analysis between the above two parameters lead to the relation: $M_0 f_c^3$ = (2.09×10^{16}Nm/s3) for the study area. Value of E_S computed in the study varies from 1.86×10^8J–1.75×10^{12}J. Further, value $\Delta\sigma$ of σ_A is found varying from 0.65MPa–21.13MPa while σ_A is found in the range of 0.07MPa–2.76MPa. It is observed that both $\Delta\sigma$ and σ_A approximately follow the theoretical relation as; σ_A=0.23$\Delta\sigma$. Another outcome of the study is the site amplification curves developed based on the GINV results of horizontal and vertical components for all the recording stations. Further, site transfer function (STF) for all the recording stations characterised by the ratio of horizontal and vertical site amplification components is computed and, amplification function (A_{peak}) and predominant frequency (f_{peak}) are determined. Comparison of estimated STFs based on GINV and results of Horizontal to Vertical Spectral Ratio method (HVSR) show similarity in terms of the f_{peak} values.

1. INTRODUCTION

The north–west Himalaya and its foothills within India encompassing the states of Jammu and Kashmir, Himachal Pradesh, Uttarakhand, Punjab, Haryana and national capital of India, New Delhi is home for about 96 million people as per 2011 Census. This is one of the fastest growing regions in the entire Himalayan belt with respect to population growth due to rapid urbanization. Records of seismic activities suggest that the above area represents an active tectonic region experiencing frequent damage inducing EQs. High seismicity of this region is because of continuous subduction of the Indian plate under the Eurasian plate [Gansser, 1964]. Major Seismotectonic features in this region is mainly defined by three north–dipping thrusts namely; the Main Central Thrust (MCT), the Main Boundary Thrust (MBT) and the Himalayan frontal Thrust (HFT) [Valdiya, 1984]. Both the MCT and the MBT are produced during the Cenozonic shortening [Valdiya, 1984;

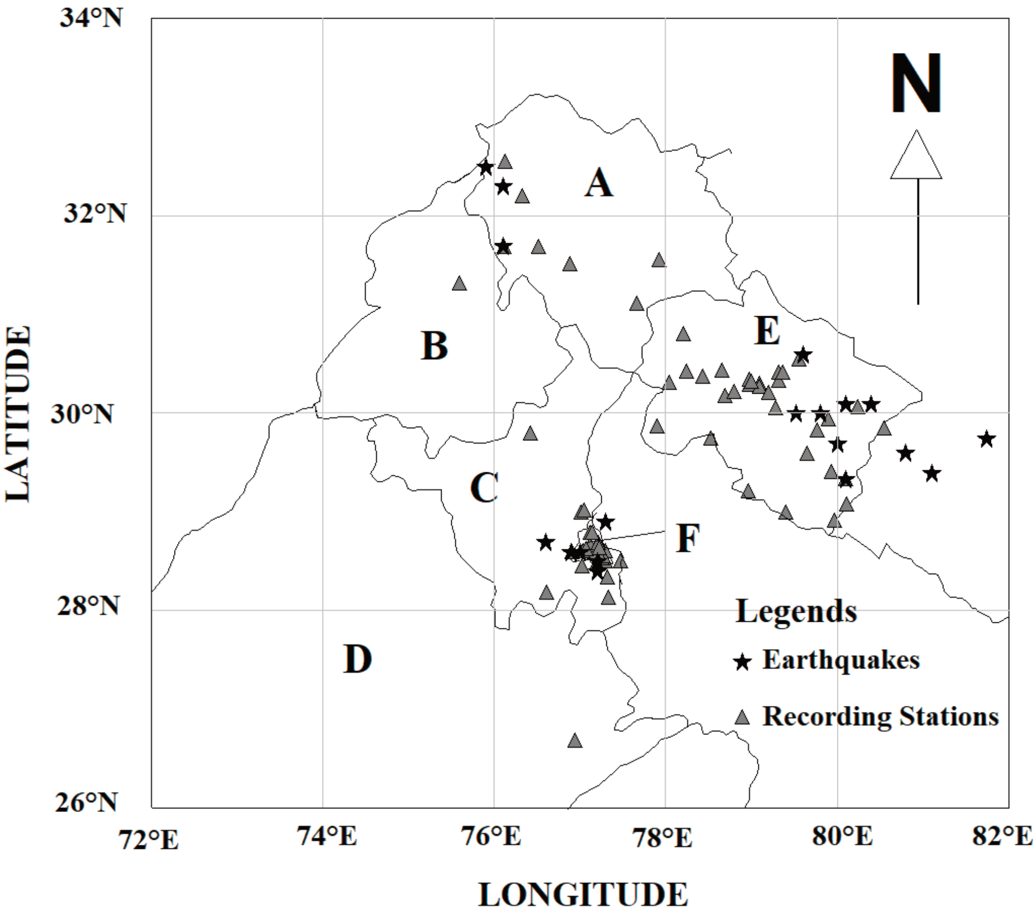

FIGURE 1. Map of the region under study with location of EQs (stars) and recording stations (triangles). Note: A– Himachal Pradesh, B–Punjab, C–Haryana, D–Gujarat, E–Uttarakhand, F–Delhi.

				GINV		HVSR*		Site class given by Chopra et al. (2018)	Range of f_{peak} as per Alessandro et al. (2012) classification scheme
Si.No.	Station Code	Lat .(°) (N)	Lon. (°) (E)	f_{peak}	A_{peak}	f_{peak}	A_{peak}		
1	2	3	4	5	6	7	8	9	10
			Uttarkhand						
1	ALM	29.6	79.7	2.1	3.0	2.8	4.4	VI	–
2	BAG	29.8	79.8	1.5	4.7	1.5	5.2	VII	–
3	BAR	30.8	78.2	3.0	4.5	2.8	7.0	II	2.5 Hz ≤ f_{peak} ≤ 5 Hz
4	CHA	32.6	76.1	3.6	2.4	2.0	2.9	III	1.66 Hz ≤ f_{peak} ≤ 2.5 Hz
5	CHP	29.3	80.1	5.4	5.2	5.6	6.5	I	f_{peak} >5 Hz
6	DHA	29.8	80.5	3.1	3.3	2.7	5.5	VII	–
7	DNL	30.4	78.2	2.8	3.3	2.0	7.1	IV	f_{peak} < 1.66 Hz
8	DUD	30.3	78.0	2.9	5.8	3.1	7.1	II	2.5 Hz ≤ f_{peak} ≤ 5 Hz
9	GAR	30.1	79.3	2.4	3.4	2.3	4.5	III	1.66 Hz ≤ f_{peak} ≤ 2.5 Hz
10	GHA	30.4	78.7	5.2	2.3	4.5	5.5	VI	–
11	GLTR	30.3	79.1	2.9	3.5	2.8	6.1	–	–
12	JSH	30.5	79.6	1.4	2.2	1.5	3.0	VII	–
13	KAP	29.9	79.9	3.7	6.4	3.3	9.2	II	2.5 Hz ≤ f_{peak} ≤ 5 Hz
14	KHA	28.9	80.0	1.3	4.2	2.0	8.0	VI	–
15	KOT	29.7	78.5	0.7	2.4	0.7	3.3	VII	–
16	KSK	29.2	79.0	3.1	3.8	3.2	9.9	–	–
17	MUN	30.1	80.2	4.3	2.8	7.0	3.6	V	–
18	PTI	29.4	79.9	4.0	6.6	3.6	8.0	II	2.5 Hz ≤ f_{peak} ≤ 5 Hz

19	ROO	29.9	77.9	1.2	3.0	1.3	5.2	VI	–
20	RUD	30.3	79.0	1.3	2.8	1.5	4.2	V	–
21	TAN	29.1	80.1	5.4	3.4	5.0	6.3	II	2.5 Hz ≤ f_{peak} ≤ 5 Hz
22	THE	30.4	78.4	1.6	2.0	1.5	3.6	VI	–
23	UDH	29.0	79.4	2.7	6.9	2.2	10.1	II	2.5 Hz ≤ f_{peak} ≤ 5 Hz
24	GDRI	30.2	78.7	6.0	2.0	5.1	4.8	–	–
25	TLWR	30.3	79.0	1.1	2.1	1.0	4.6	–	–
26	UKMB	30.3	79.1	1.0	2.9	1.4	10.0	–	–
27	NUTY	30.2	79.2	4.8	2.4	4.7	4.3	–	–
28	STRK	30.3	79.0	4.7	2.8	4.7	5.8	–	–
29	NANP	30.3	79.3	3.9	3.5	3.8	9.1	–	–
			Himachal Pradesh						
1	AMB	31.7	76.1	1.7	4.3	1.2	9.3	VII	–
2	BHA	31.6	77.9	4.5	3.0	4.1	4.4	II	2.5 Hz ≤ f_{peak} ≤ 5 Hz
3	CHM	30.4	79.3	1.4	5.4	1.5	7.5	I	–
4	DHH	32.2	76.3	2.7	3.0	2.7	4.9	II	2.5 Hz ≤ f_{peak} ≤ 5 Hz
5	HAM	31.7	76.5	2.9	3.3	3.1	6.6	VII	–
6	JUB	31.1	77.7	5.8	3.3	5.6	4.9	VII	–
7	SND	31.5	76.9	5.0	3.0	5.0	4.2	VI	–
8	HGR	26.7	76.9	2.3	4.0	2.0	7.0	–	–
			Haryana						
1	PAL	28.1	77.3	2.8	2.7	2.9	3.4	VI	–
2	JAFR	28.6	76.9	6.0	2.0	7.1	2.6	I	f_{peak} >5 Hz
3	GUR	28.4	77.0	1.0	4.1	1.0	5.2	V	–
4	REW	28.2	76.6	2.5	2.1	2.5	3.7	–	–
5	SON	29.0	77.0	1.0	3.5	2.8	4.0	VI	–
6	ROH	28.6	77.2	1.4	3.1	2.0	4.6	IV	f_{peak} < 1.66 Hz
7	CRRI	29.0	77.1	4.3	3.5	4.4	9.3	–	–
8	BAL	28.3	77.3	1.5	3.0	1.4	5.8	VI	–
9	KAI	29.8	76.4	1.2	3.0	1.2	6.5	VI	–
10	PLW	28.13	77.33	2.4	2.9	2.3	4.4	–	–
11	NOI	28.507	77.479	2.3	3.8	2.3	10.4	III	1.66 Hz ≤ f_{peak} ≤ 2.5 Hz
			Punjab						
1	JAL	31.3	75.6	2.9	1.2	2.9	1.7	–	–
			Delhi						
1	IGN	28.5	77.2	3.6	2.6	4.5	3.9	–	–
2	DJB	28.7	77.2	2.2	3.2	10.0	4.5	V	–
3	IMD	28.7	77.2	6.0	2.0	6.3	2.9	–	–
4	NTPC	28.5	77.3	2.8	3.6	2.8	5.4	–	–
5	ANC	28.5	77.3	4.6	3.2	4.5	4.5	–	–
6	JAMI	28.6	77.3	4.7	3.2	4.5	7.3	–	–
7	LDR	28.6	77.2	0.7	4.3	0.9	7.0	I	f_{peak} < 1.66 Hz
8	VCD	28.6	77.2	4.6	2.7	4.6	3.6	–	–
9	IIT	28.6	77.3	4.3	2.9	4.5	4.3	–	–
10	NSIT	28.6	77.0	2.4	2.5	2.3	3.9	–	–
11	RGD	28.7	77.1	2.3	2.1	2.9	3.8	–	–
12	DLU	28.7	77.2	1.8	2.0	1.9	3.7	I	f_{peak} < 1.66 Hz
13	DCE	28.8	77.1	3.8	3.1	4.7	4.2	–	–
14	IGI	28.6	77.1	2.2	2.4	2.2	3.8	–	–
15	ZAKI	28.6	77.2	3.9	3.5	3.9	8.4	–	–
16	ALIP	28.8	77.1	2.3	3.2	2.5	6.9	–	–
17	CNDB	30.2	78.8	1.4	3.1	2.0	4.6	–	–
18	CNKB	30.4	79.4	2.1	3.8	2.0	4.5	–	–

** Harinarayan and Kumar (2018a)*

TABLE 1. Detail of strong motion recording stations.

Malik and Nakata, 2003]. The HFT is the youngest active thrust separating the Himalaya region and the Indo–Gangetic alluvial plain [Kumar et al., 2009]. Continuous thrusting along the MCT, HFT and MBT have produced major EQs in north–west Himalaya [Philip et al., 2014]. Two major EQs occurred in the past 120 years in this region include the 1905 Kangra–Himachal Pradesh EQ (M_S=7.8) [Ambraseys and Douglas, 2004] and the 2005 Muzzafarbad–Kashmir EQ (M_W=7.6) (Avouac et al. 2006). The above mentioned EQs had left behind a trail of severe loss of lives and infrastructure. Bhattacharya and Kayal [2005] reported the source zone of the 1905 Kangra EQ to be beneath the Himalayan Frontal Fault, south of the MBT. 1905 Kangra EQ killed 20,000 people [Wallace et al., 2005] and caused a 15 cm uplift in the region of Dehra Dun, located 250 km from the epicentre, [Burrard, 1910a, b]. 2005 Muzzafarbad EQ killed about 82,000 people in Kashmir and caused wide spread slope failures in Neelum, Jhelum, and Kunhar valleys. [Aydan et al., 2009]. Recent EQs including the 1991 Uttarkashi (Mw=6.8) and the 1999 Chamoli (Mw=6.6) occurred in the MCT zone [Harbindu et al., 2014]. The 1991 Uttarkashi EQ killed 760 people (Kayal, 2001) and caused huge damages to buildings in Uttarkashi district (Kumar and Mahajan, 1994). The 1999 Chamoli EQ caused landslides in Gopeshwar town, located less than 2km northwest of Chamoli city [Sarkar et al., 2001] and produced tremors in locations like Chandigarh and Delhi, located far away from the epicentre [Mundepi et al., 2010]. It has to be highlighted here that IS 1893: 2016 classifies the entire north–west Himalaya region as seismic zone IV and V, indicating regions of high to very high seismic activity.

It has been widely acknowledged that ground motion at a certain site during an EQ is a collective function of site, path and source parameters (jointly referred to as EQ parameters). Site parameters accounts for the modification of incoming seismic waves characteristics (amplitude, frequency content and duration) by subsurface soil medium. Similarly, path parameters constitute geometric spreading and anelastic attenuation which account for the attenuation of seismic waves as travel away from the source through the crustal medium. On the other hand, source parameters include M_0 (defined as the measure of the size of seismic disturbance), E_S (defined as wave energy that would be released if an EQ happened in an infinite medium without energy loss) and $\Delta\sigma$ (defined as the measure of change in the average state of stress before and after rupture). Knowledge about region specific EQ parameters is important for seismic hazard assessment, especially those using physical models [Hassani et al., 2011]. Widely used approach to estimate EQ parameters in Fourier amplitude is to apply generalized inversion (GINV) method to the recorded EQ data. GINV was introduced by Andrews, (1986) after modifying the standard spectral ratio method [Borcherdt, 1970] into a generalised inversion problem. Authors worldwide have used this method on seismic records to estimate EQ parameters [Castro, 1990; Boatwright et al., 1991; Harinarayan and Kumar, 2018b,c].

Previously, Harinarayan and Kumar, [2019] had evaluated path attenuation parameters and site characteristics for regions in and around the north–west Himalaya using a two–step non–parametric–non–reference site GINV technique. However, estimation of source parameters was not attempted by Harinarayan and Kumar, [2019]. In the current study, ground motions corresponding to 21 EQs happened between the years 2004 and 2017, are analysed in the frequency range of 0.25 Hz to 15 Hz for estimating source and site spectra simultaneously using GINV. Obtained source spectra from the horizontal component of ground motion (calculated as the root mean square average of the east–west and north–south components) is then interpreted using the point source model [Brune, 1970] to determine source parameters like M_0 and f_c. Further, relationships between above source parameters, termed as scaling relations, are developed for the region under study. Scaling relations give parameters such as E_S, $\Delta\sigma$ and σ_A, which are required for scenario EQ simulation as well as development of regional attenuation relations. Further, site amplification for the horizontal and the vertical component is determined, and STF is estimated as the ratio of horizontal to vertical site amplification. Finally, the STF for each of the recording stations obtained using GINV in the present study is compared with HVSR estimates developed similar to Chopra et al. 2018 and Harinarayan and Kumar, 2018a.

2. STRONG MOTION DATA SET

EQ data used in this work is obtained from PESMOS (Program for Excellence in Strong Motion Studies) database, which consist of accelerograms from recording stations installed during or after 2004 as part of a project titled “National Strong Motion Instrumentation Network”. EQs are recorded using internal AC–63 GeoSIG triaxial force balanced accelerometers attached with external GPS [Kumar et al., 2012]. Information regarding the instrumentation can be found on the PESMOS website (http://www.pesmos.in/).

EQ records from PESMOS database, for the region in and around the north-west Himalaya, are considered here. While selecting ground motion records, EQs with at least three recordings available, are considered for further analyses. Thus, final database used in the present study consists of 156 three components accelerograms from 21 EQs, recorded at 78 stations, located widespread across the study area. The range of M for the database varies from 2.5 to 5.7 with H ranging from 5 to 39.3km. Location details of each of the recording station, used in the current study are summarized in Table 1. Details of EQs including the M and epicentre coordinates are listed in Table 2. In addition, Fig. 1 shows the location of the recording stations and EQs used for inversion.

2.1 DATA PROCESSING

For inversion analysis, EQ records are subjected to baseline correction with a 5% cosine taper followed by band-pass Butterworth filter in the frequency range of 0.25Hz and 15Hz. Further, S wave part of each accelerogram is selected as the time windows beginning from 0.5s before the starting of the S wave and ending when 90% of the total energy of the EQ record is reached [Bindi et al., 2009]. In addition, the time windows for EQ records vary from 4 to 15s. The maximum window length is restricted to 15s in order to avoid records having too much Coda wave energy [following Oth et al., 2008]. Further, the Fourier amplitude spectra (FAS) are calculated for S wave portion of the EQ record. Obtained FAS is then smoothened as per Konno and Ohmachi (1999) algorithm with a smoothing parameter b = 20. Further, source and site spectra are generated simultaneously using an inversion procedure as discussed in Section 3.

3. GENERALIZED INVERSION METHOD

The smoothened FAS $U_{ij}\,(f,R_{ij})$ at a recording station i, from source j with M and hypocentral distance R can be expressed in frequency domain (f) following Castro, (1990) as;

$$U(f)_{ij} = S(f)_j \, P(f,R_{ij})_{ij} \, G,(f)_j \tag{1}$$

Here, $S(f)_j \, P(f,R_{ij})_{ij}$ and $G,(f)_j$ denote the source spectrum, path attenuation component and site term respectively. Later, the path attenuation component is removed from $U(f)_{ij}$ in accordance with Andrews [1986] as;

$$U^A(f)_{ij} = \frac{U(f)_{ij}}{P(f,R_{ij})_{ij}} = S(f)_j \;\; G,(f)_j \tag{2}$$

The value of $P_{ij}(f,R_{ij})$ includes the effects of anelasticity of heterogeneous media and geometric spreading, which as per Castro, (1990) can be determined using the following expression;

$$P(f)_{ij} = \frac{1}{R_{ji}} \left[e^{\frac{(-(\pi\, f\, R_{ji})}{(Q_S(f)\,\beta)}} \right] \tag{3}$$

In eq. 3, $Q_S(f)$ is the quality factor for S wave and β is the average shear wave velocity of the crustal medium for the region considered as 3.5km/s as per Mukhopadhyay and Kayal, (2003). Value of $Q_S = 105f^{0.94}$ as given by Harinarayan and Kumar, [2018c] for the region in and around the north-west Himalaya is used in this work. Eq. 2 is linearized by taking natural logarithms as follows;

$$InU^A(f)_{ij} = In\,S(f)_j + In\,G(f)_i \tag{4}$$

According to Andrews, [1986], an undetermined degree of freedom between source and site term exists in eq. 4 that can be resolved by using constrained site spectral function in the inversion [Castro et al., 1990], by setting the average of site spectra of a set of recording stations located on rock site (termed as reference sites) to unity, for the entire frequency range. Reference sites are carefully selected, since site and source terms in the inversion are related to the imposed site constraint. Any discrepancies in the reference site condition would lead to a systematic bias in the source spectra [Oth and Kaiser, 2014]. Identifying reference sites in PESMOS based recording stations is a challenging task because of lack of accurate site class information. For this reason, reference stations are chosen based on the results of HVSR study by Hari-

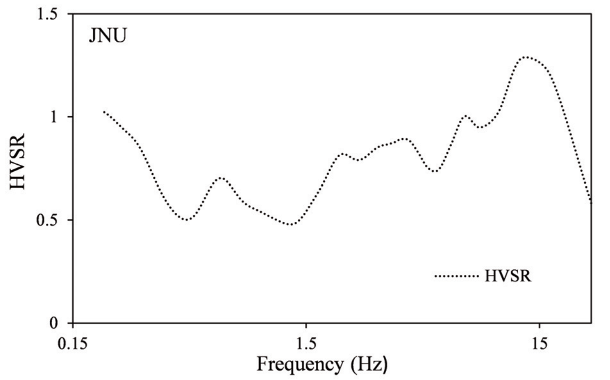

FIGURE 2. HVSR curve for JNU recording station (Harinarayan and Kumar 2018a).

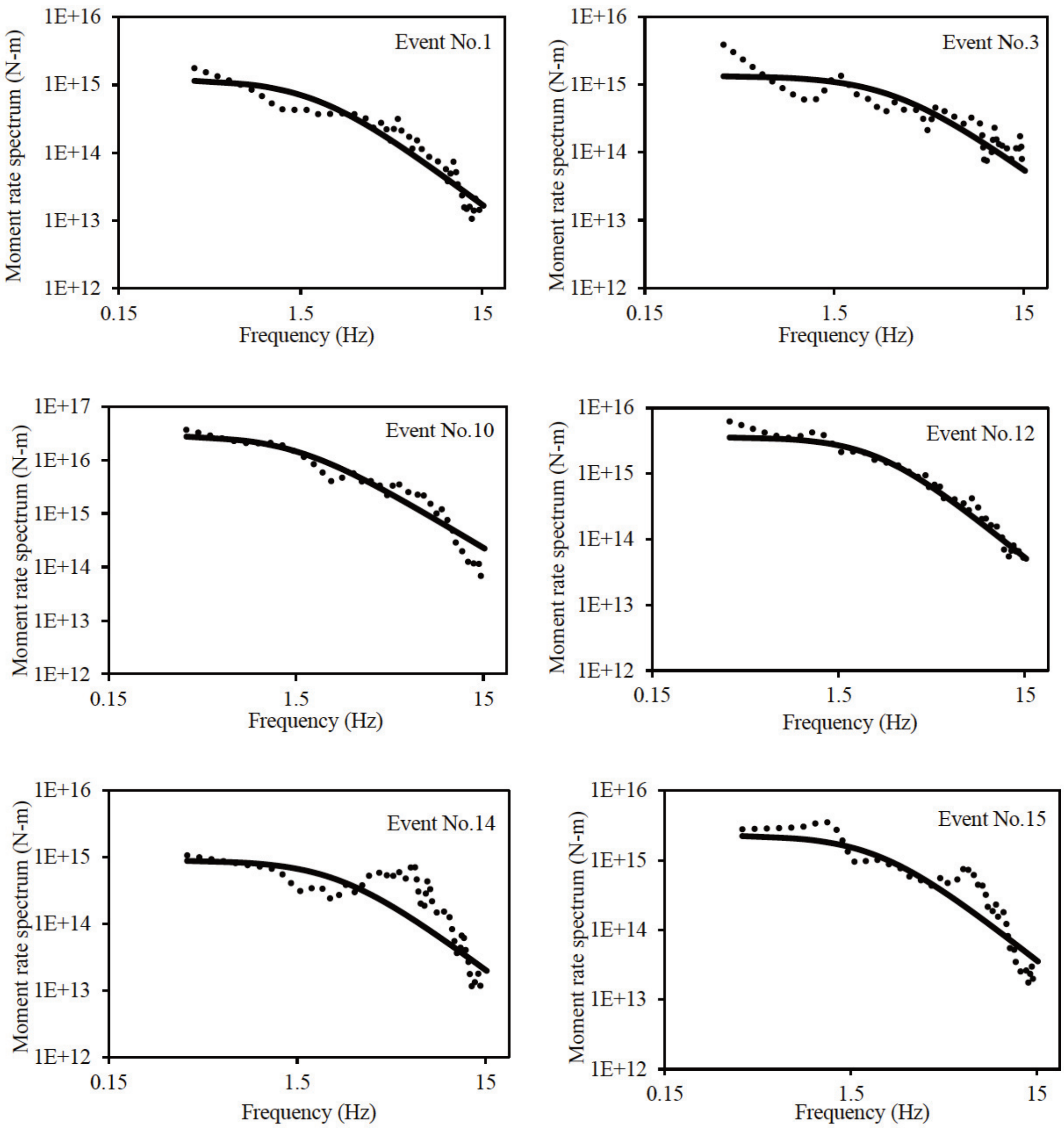

FIGURE 3. The computed (dotted line) and the best–fit (thick line) moment rate spectra.

narayan and Kumar, [2018a]. Figure 2 shows an example of site amplification curves for reference station in JNU based on HVSR [Harinarayan and Kumar, 2018a] results.

A flat response curve throughout the frequency range, with amplification value close to 1.0 can be observed in Figure 2. Complete list of reference stations used for the present work is presented in Table 1.

Eq. 4 constitute a system of linear equations of the form $Ax = b$ where x is the model vector matrix, A is the system matrix, and b is the data vector which includes $InU^A(f)_{ij}$ and constrained reference site amplification values. Eq. 4 in this work is solved to obtain source and site spectrum using Singular value decomposition algo–rithm in a least square sense for each frequency follow–ing Menke, [2018].

4. RESULTS

Earlier discussed source and site spectrum are esti–mated here using the inversion procedure discussed in the preceding section. Results of the inversion are dis–cussed below.

4.1 SOURCE PARAMETERS

The source spectrum, $S(f)_j$ of all the 21 EQ events obtained from inversion is shown in Fig. 3 (indicated by dashed line). In order to estimate source parameters, each source spectrum is compared and fitted to point source model of Brune, [1970] as discussed below;

The obtained source spectra $S(f)_j$, of the j^{th} EQ event, from the inversion is expressed as (Brune, 1970);

Event No.	Date (dd–mm–yyyy) (hh:mm)	Lat. (°) (N)	Lon. (°) (E)	Depth (Km)	Magni–tude	M_0 (N–m)	f_c (Hz)	ϒ	r (m)	Δσ (MPa)	E_s (J)	σ_A (MP)
−1	−2	−3	−4	−5	−6	−7	−8	−9	−10	−11	−12	−13
1	25–11–2007 (23:12)	28.6	77.0	20.3	4.3	1.2E+15	1.8	2.0	703.8	1.5	5.67E+09	.2
2	19–08–2008 (10:54)	30.1	80.1	15.0	4.3	3.45E+14	2.3	2.4	550.8	0.9	5.61E+08	0.1
3	31–01–2009 (03:07)	32.5	75.9	10.0	3.7	1.35E+15	3.1	2.0	408.7	8.7	3.46E+10	1.1
4	04–09–2008 (12:53)	30.1	80.4	10.0	5.1	1.08E+15	2.0	2.0	633.4	1.9	6.19E+09	0.3
5	17–07–2009 (11:07)	32.3	76.1	39.3	3.7	1.60E+15	3.7	2.5	342.4	17.4	5.24E+10	1.4
6	11–01–2010 (05:15)	29.7	80.0	15.0	3.9	3.53E+14	4.0	2.5	316.7	4.9	6.39E+09	0.8
7	24–02–2010 (19:20)	28.6	76.9	17.0	2.5	4.96E+13	5.5	2.0	230.3	1.8	1.86E+08	0.2
8	14–03–2010 (6:53)	31.7	76.1	29.0	4.6	5.50E+14	2.6	2.1	487.3	2.1	3.01E+09	0.2
9	31–05–2010 (11:37)	30.0	79.8	10.0	3.6	1.19E+15	4.0	3.0	316.7	16.4	3.01E+10	1.1
10	04–04–2011 (11:31)	29.6	80.8	10.0	5.7	2.91E+16	1.5	2.1	844.6	21.1	1.75E+12	2.7
11	12–03–2012 (22:07)	28.9	77.3	5.0	3.5	6.80E+14	3.3	1.4	383.9	5.3	1.87E+11	1.2
12	05–03–2012 (07:41)	28.7	76.6	14.0	4.9	3.60E+15	2.4	2.3	527.9	10.7	8.65E+10	1.1
13	11–11–2012 (18:39)	29.3	80.1	5.0	5.0	1.80E+15	2.1	2.0	603.3	3.6	1.97E+10	0.5
14	02–01–2013 (17:42)	29.4	81.1	10.0	4.8	9.00E+14	2.5	2.1	506.8	3.0	7.22E+09	0.4
15	09–01–2013 (07:44)	29.8	81.7	5.0	5.0	2.30E+15	2.1	2.1	603.3	4.6	2.88E+10	0.6
16	11–11–2013 (19:11)	28.5	77.2	10.0	3.1	7.10E+13	3.5	1.5	362.0	0.7	2.03E+08	0.1
17	11–11–2013 (22:10)	28.4	77.2	11.0	2.8	8.10E+13	4.6	2.0	275.4	1.7	3.22E+08	0.2
18	11–11–13 (20:11)	28.4	77.2	13.0	3.1	1.92E+14	3.3	1.6	383.9	1.5	8.16E+08	0.2
19	29–11–2015 (02:47)	30.6	79.6	15.0	4.0	8.99E+14	3.6	3.0	351.9	9.0	3.26E+10	1.6
20	25–09–2016 (21:41)	30.0	79.5	11.0	3.7	7.19E+14	3.6	3.0	351.9	7.2	8.05E+09	0.5
21	01–12–2016 (16:52)	30.6	79.6	19.0	3.3	6.91E+15	2.2	3.0	575.9	15.8	4.33E+11	2.8

TABLE 2. List of source parameters determined in this study.

$$S(f)_j = \left[4\pi^2 f^2 (R_\emptyset) VF \Big/ (4\pi\rho\beta^3 R_0) \right] \ddot{M}_{0J} \tag{5}$$

In eq. 5, $R_\emptyset$ =0.55 (Mandal and Dutta, 2011), is the average shear wave radiation pattern; F=2 [Zafarani et al., 2012] represents the free surface amplification; V = $1/\sqrt{2}$, accounts for the partition of S wave energy into two horizontal components; ρ=2.8g/cm^3 and β=3.5km/s denote the mass density and the shear wave velocity in the vicinity of the EQ source [Mandal and Dutta, 2011]; R_0 =1km is a reference distance and $\ddot{M}_{0J}$ represents the moment rate spectrum. Rearranging the terms of eq. 5 gives;

$$\ddot{M}_{0J} = \frac{S(f)_j}{\left[4\pi^2 f^2 (R_\emptyset) VF \Big/ (4\pi\rho\beta^3 R_0) \right]} \tag{6}$$

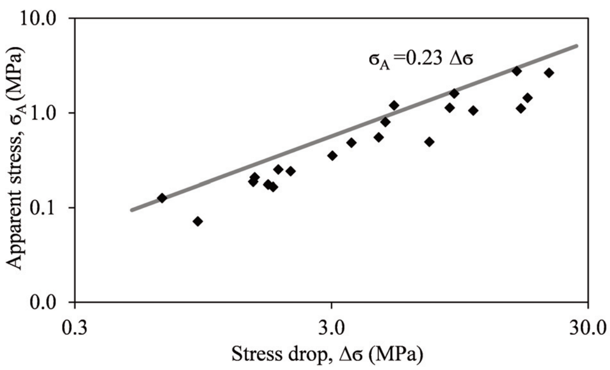

FIGURE 4. Stress drop versus apparent stress. The theoretical relation given by Kikuchi and Fukao, 1988 is indicated by solid line.

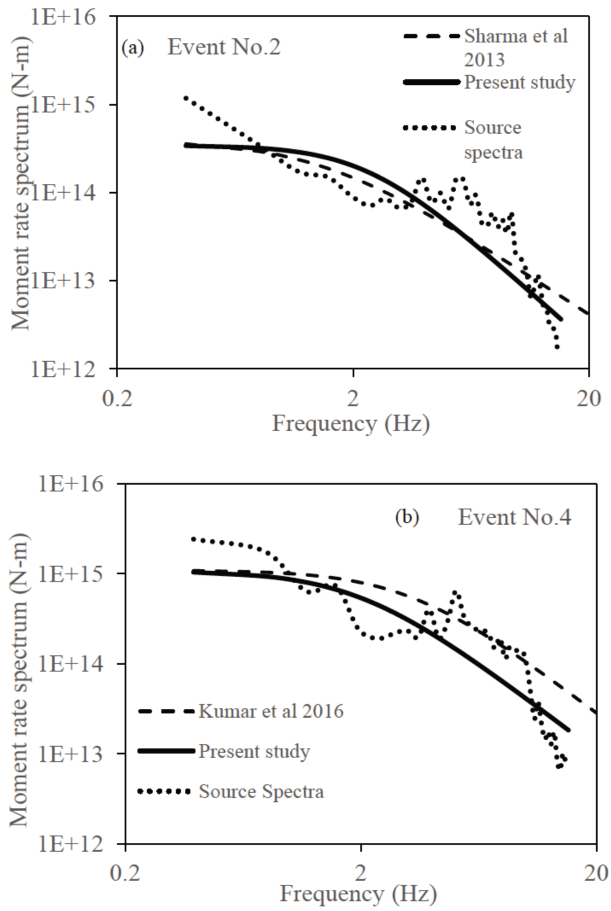

FIGURE 5. Comparison of the estimated source parameters obtained in the present study with those reported by a) Sharma et al. 2013 b) Kumar et al. 2016.

$\ddot{M}_{0J}$ of 21 EQ events, based on $S(f)_j$, obtained in inversion, is computed using eq. 6 as shown in Fig. 3. Further, $\ddot{M}_{0J}$ of each EQ event is compared and fitted to the theoretical model given in eq. 7 [after Brune, 1970] in order to estimate source parameters.

$$\ddot{M}_{0J} = \frac{M_0}{1+(f/f_{cj})^{\Upsilon}} \tag{7}$$

A nonlinear least square approach (similar to Bindi et al. 2009) is adopted here to determine the values of M_0, f_c and Υ for each EQ event, based on $\ddot{M}_{0J}$ values in eq. 7. The values of M_0, f_c and Υ obtained in the present study are tabulated in Table 2 column 7, 8 and 9 respectively. Value of M_0 as obtained from the analysis ranges between 4.96×10^{13}Nm to 2.91×10^{16}Nm. Further, the value of f_c is found in the range of 1.5Hz to 5.5Hz while the value of Υ is in the range of 1.4 to 3. An excellent fit between the theoretical $\ddot{M}_0$ (obtained by substituting the values of M_0, f_c and Υ in eq. 7) and the computed $\ddot{M}_0$ as observed in Figure 3 indicates the robustness of the above estimated source parameters. Afterwards, $\Delta\sigma$, E_S, and σ_A for each of the 21 EQ events are computed as discussed below.

$\Delta\sigma$ for each of the 21 EQ event are computed using eq. 8 below, based on the above determined M_0, and f_c values and assuming a circular fault of radius r, in accordance with the theoretical source model of Brune, [1970].

$$\Delta\sigma = \left({}^{7M_0}\!/_{16r^3} \right) \times 10^{-6} \tag{8}$$

Where,

$$r = {}^{2.34\beta}\!/_{2\pi f_c} \tag{9}$$

In eq. 8 and 9, r, β, M_0, and $\Delta\sigma$ have units of m, m/s, Nm and MPa respectively. Values of r and $\Delta\sigma$ are tabulated in Table 2, columns 11 and 13 respectively. Value of r falls between 230.34m and 844.60m for 21 events, with an average of 457.5m. Similarly, the value of $\Delta\sigma$ vary from 0.53MPa to 21.13MPa, with an average of 6.43MPa for 21 events. Note, while most of the events have lesser than 10 MPa only 5 events (events 5, 9, 10, 12 and 21) have $\Delta\sigma$ greater than 10 MPa. Further, S wave energy (E_S) associated with each event is estimated in the frequency range 0.25Hz –15Hz in accordance to the relation (eqs. 10, 11), given by Vassiliou and Kanamori, [1982].

$$E_S = A \int_{-\infty}^{+\infty} |2\pi f \ddot{M}_{0J}|^2 \, df \tag{10}$$

Where,

$$A = (15\pi\rho\alpha^5)^{-1} + (\pi\rho\beta^5)^{-1} \tag{11}$$

Where, α is the P wave velocity at the source region, taken as 6.4 km/s [Mandal and Dutta, 2011]. Estimated values of E_S are tabulated in Table 2, Column12. Value

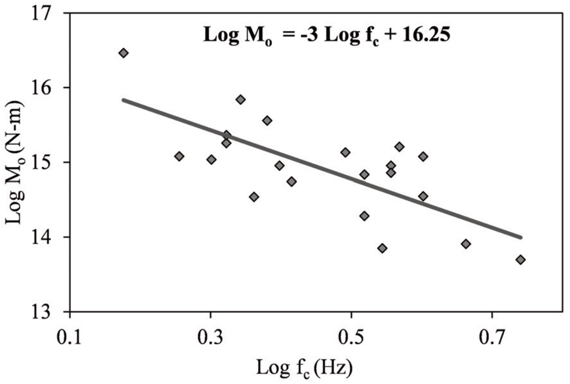

FIGURE 6. The plot of scalar moment versus corner frequency in logarithmic unit. The regression relation is indicated by solid line.

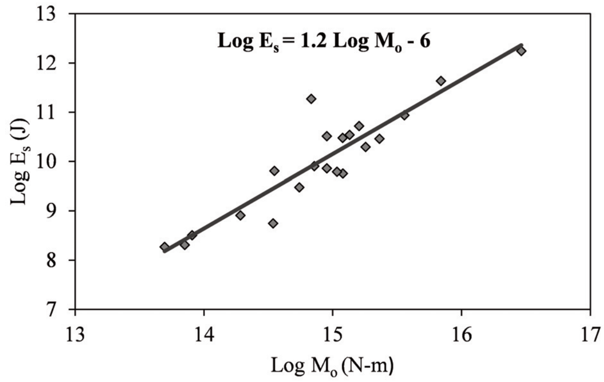

FIGURE 7. The plot of energy released versus corner frequency in logarithmic unit. The regression relation is indicated by solid line.

of E_S falls between 1.16E+07 J and 1.75E+12 J, with an average value of 1.27E+11 J for 21 events. It has to highlighted here that the value of E_S obtained in the present study is underestimated to some extent because of the frequency band limit applied in eq. 10. Based on the value of E_S estimated in the present study, apparent stress (σ_A) for each of the 21 events are estimated following Brune, [1970] as:

$$\sigma_A = \mu \, E_s/M_0 \qquad (12)$$

In eq. 12, μ is the rigidity modulus estimated using the formula: $\mu = \beta^2\alpha$. Calculated values of σ_A are tabulated in Table 2 Column 13. It can be seen from the Table 2, column 13 that the estimated σ_A in the present study is in the range of 0.07MPa to 2.76MPa, with an average of 0.81MPa for 21 events. Fig. 4 shows a comparison of σ_A, Δσ and the theoretical line, σ_A =0.23 Δσ given by Kikuchi and Fukao, [1988] represented by a solid line. It can be seen from Fig. 4 that the relation between estimated σ_A and Δσ in the present study is consistent with the theoretical relation.

4.2 COMPARISON WITH EXISTING LITERATURES

There are limited studies available where source parameters for EQs in the north-west Himalaya were determined [Sharma et al., 2013; Kumar et al., 2016; Mittal et al., 2016a, b]. Comparison of the estimated source parameters with those obtained by above researchers for EQs considered in the present study is discussed in this section. Sharma et al. [2013] analysed strong motion records from Uttarakhand region and reported values of Δσ, f_c, and r as 1.5MPa, 1.5Hz and 1000m respectively for 2008 August EQ [event no. 2, Table 2].

This is close to the value of Δσ =0.9MPa, f_c =2.3Hz and r =550.8m obtained in the present study (see Fig. 5a). In another study, Kumar et al. (2016), based on Spectral analysis using grid search technique reported values of Δσ as 4.16Mpa and 3.6Mpa for 2009 January EQ [event no. 3, Table 2] and 2008 September EQ [event no. 4, Table 2] respectively, which are in range with the Δσ estimate of 8.6MPa and 1.6MPa obtained for the same events in the present study (see Figure 5b).

Mittal et al. [2016a], using least square method estimated and as 36.2MPa and 1.19Hz respectively for 2011 Nepal Himalayan EQ [event no. 10, Table 2].

Values estimated by Mittal et al. (2016a) are close to the values obtained in the present study (Δσ =31.13MPa and f_c=1.19Hz). In another study, Mittal et al. (2016b) analysed 2012 March EQ [event no. 12, Table 2] using stochastic point source model and reported the value of Δσ and f_c as 12.4MPa and 1.78Hz respectively, which are matching with the value of Δσ =10.71MPa and f_c=2.4Hz obtained in the present work. Similarities in the results of the present study with that discussed above is encouraging considering the total independence of the methodologies used in each work including the present one.

5. EMPIRICAL CORRELATIONS

To understand the relation between M_0 and f_c in the north-west Himalaya, M_0 is plotted against f_c in logarithmic units (similar to Aki, 1967) and the regression yields the following expression:

$$\log M_0 = -3.19 \log f_c + 16.40 \qquad (13)$$

Eq. 13 indicates that with increase in f_c M_0 decreases. According to Aki, (1967), f_c follows the scaling law: $M_0 f_c^3 = constant$, indicating self-similarity in the EQ source. Following Aki, [1967], the slope is fixed to −3 and regression analysis is again carried out between M_0 and f_c in logarithmic scale, giving the following expression:

$$\log M_0 = -3 \log f_c + 16.25 \quad (14)$$

Plot for eq. 14 is indicated by solid line in Figure 6. Eq. 14 is rewritten as: $M_0 f_c^3 = (1.8 \times 10^{16}\text{Nm/s3})$ corresponding to a constant stress drop of 3.5MPa. Kumar et al. [2008] reported a relation $M_0 f_c^3 = (2.09 \times 10^{16}\text{Nm/s3})$ analysing 12 EQ events (4.5<M<7) in the Himalaya region, which is similar to the result obtained in the present study. In another study, Hassani et al. [2011] reported a relation $M_0 f_c^3 = (2.48\times10^{16}\text{Nm/s3})$ for EQs (3.5<M<7) corresponding to a constant Δσ of 4.9MPa for Iran. Dutta et al. (2003) obtained a relation $M_0 f_c^3 = (2.09 \times 10^{16}\text{Nm/s3})$ for EQs ($3<M_L<6.3$) corresponding to a constant Δσ of 2MPa for the anchorage area of Alaska. Findings from above mentioned studies are comparable to those obtained in the present study.

The relation between E_S and M_0, obtained in the present analysis is shown in Figure 7 and can be linearly expressed in logarithmic scale as;

$$\log E_S = 1.2 \log M_0 - 6 \quad (15)$$

In similar study, Zafarani et al. [2012] reported a relation; $\log E_S = M_0 - 4.08$ for EQs ($4<M_w<7.4$) in the Alborz Zone of Iran which is similar to the relation obtained in the present study.

The variation of Δσ with M_0, shown in Figure 8 illustrate that Δσ do not exhibit significant variation with M_0. Similarly Fig. 9 shows lack of dependence of Δσ with M. The significant lack of dependence of Δσ with M_0, and M along with the cube root scaling of f_c (in eq. 13) collectively indicates that the EQs in the north–west Himalaya follow the self–similarity process. A similar observation is reported by Kumar et al. [2016] for EQs ($3.4<m_b<5.8$) in the north–west Himalaya.

6. SITE PARAMETERS

After estimating source parameters, site amplification curves for horizontal and vertical components are developed separately using GINV. Figure 10 depicts typical amplification curves obtained for horizontal (indicated by dotted lines) and vertical (indicated by solid lines) components at 4 stations. It can be seen from Figure 10 that the obtained amplification value for horizontal component is greater than vertical component. In general, for several recording stations, clear and well defined peak in the amplification curve is observed (see Figure 10). Moreover, the frequency corresponding to the maximum amplification for the vertical and the horizontal components are matching with each other. Further, STF is computed based on the GINV results as the ratio of horizontal component to vertical component of site amplification terms for each recording station. The frequency corresponding to the maximum value of STF (denoted as A_{peak}) is termed as f_{peak}. The values of f_{peak} and A_{peak} are given in Table 1, Columns 5 and 6 respectively. Maximum value of f_{peak} of 6Hz is observed for the recording station JAFR with A_{peak} of 2. Maximum value of A_{peak} of 6.9 for UDH recording station is observed at 2.7Hz. Range of A_{peak} varies between 2 and 6.9, while the range of f_{peak} varies between 0.7Hz and 6Hz.

Above computed STF curves based on GINV are later compared with HVSR based site amplification curves estimated for the same recording stations by Harinarayan and Kumar, [2018a] and Chopra et al. [2018]. Detailed description on HVSR methodology is given in Harinarayan and Kumar, [2018a] and Chopra et al. [2018] and is not discussed in the present study.

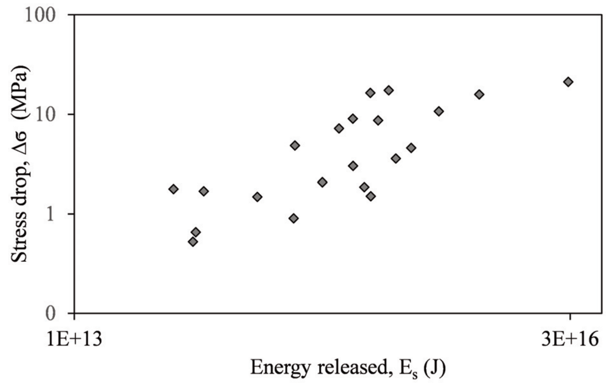

FIGURE 8. The plot of stress drop versus seismic energy.

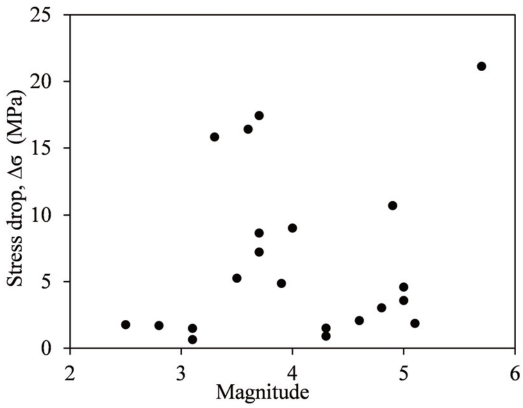

FIGURE 9. The plot of stress drop versus magnitude.

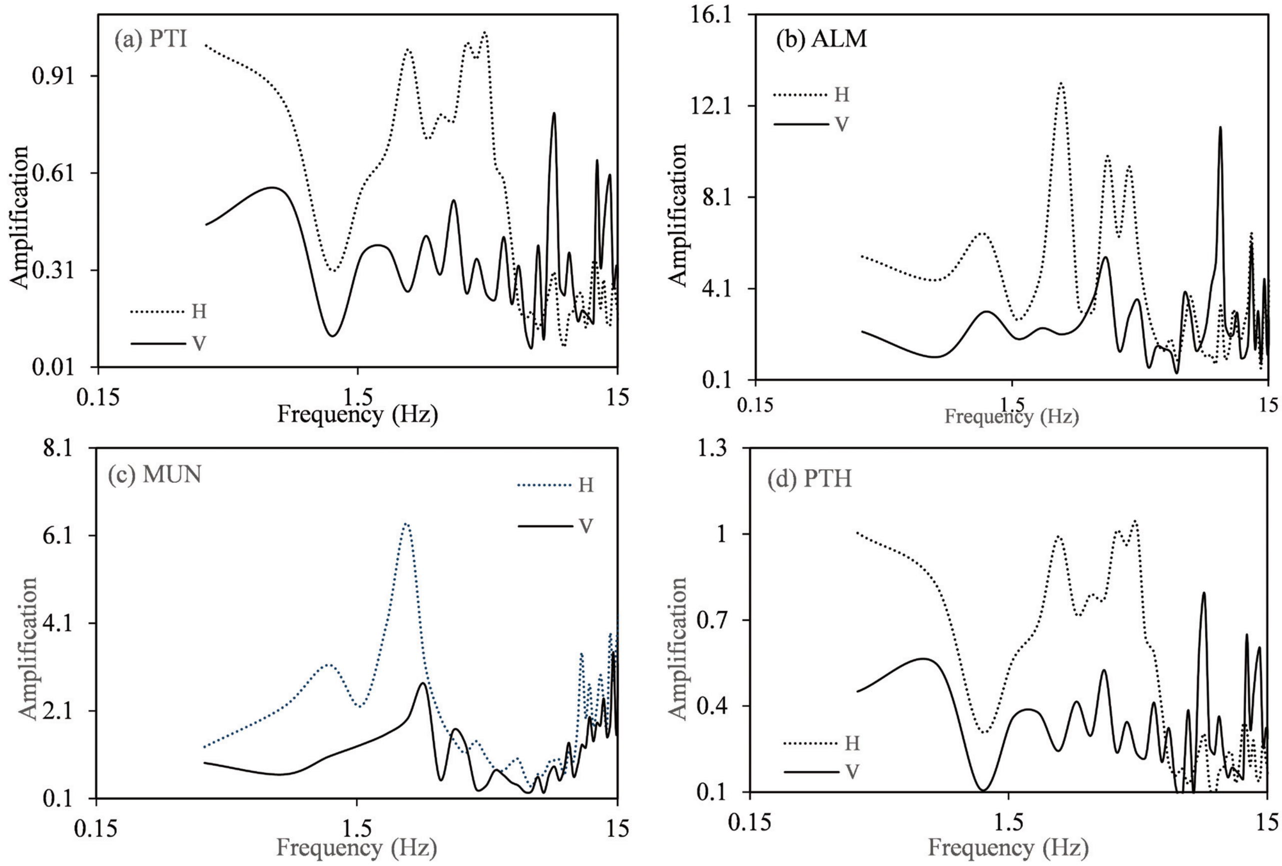

FIGURE 10. Site amplification curves obtained using GINV for horizontal component (H) and vertical component (V).

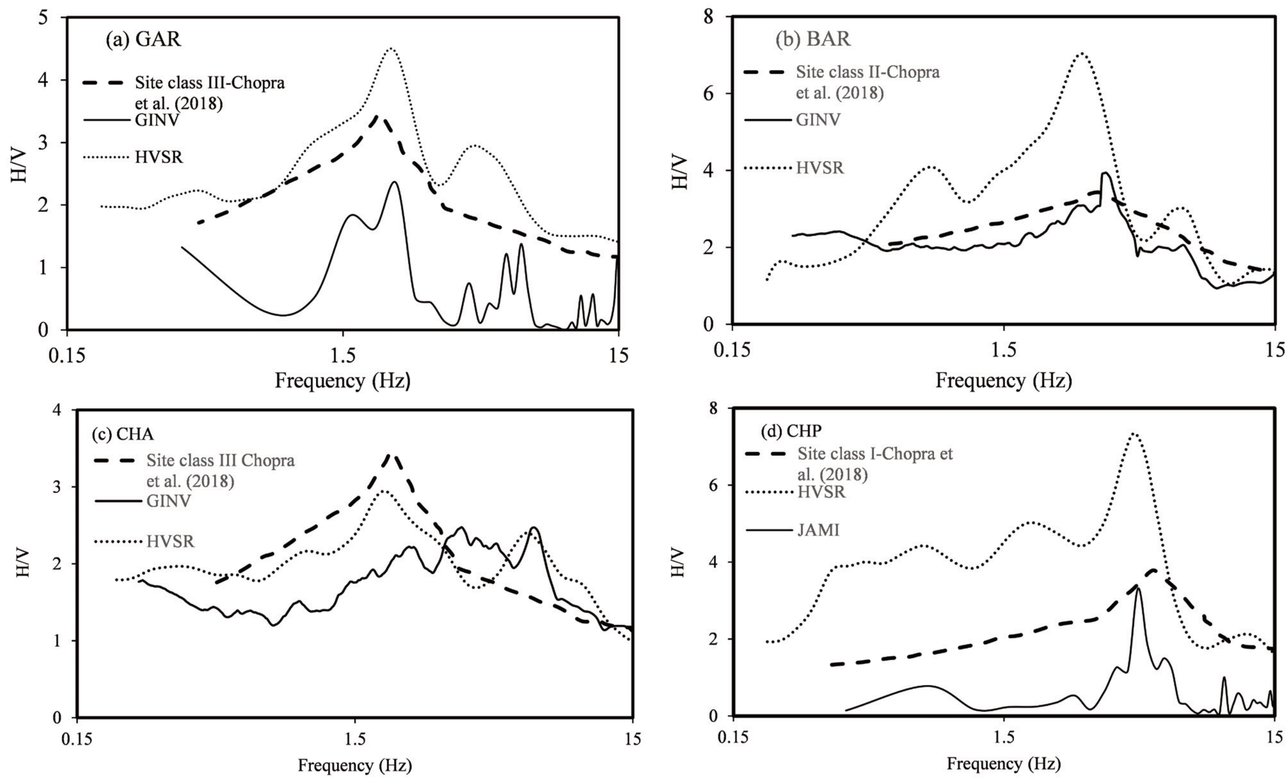

FIGURE 11. Horizontal to vertical ratio curve obtained using GINV and HVSR method.

The values of A_{peak} and f_{peak} based on HVSR analysis reported by Harinarayan and Kumar, [2018a] are listed in Column 7 and 8 respectively of Table 1. Figure 11 shows the comparison of results of HVSR (indicated by dotted lines) and GINV (indicated by solid line) for 4 typical recording stations considered in the present study. It can be concluded that both HVSR and STF based curves show similar patterns in terms of the general shape for all the recording stations. Further, overall value of f_{peak} obtained using GINV and HVSR exhibit 1:1 match at all the recording stations. A difference in terms of A_{peak} values between the curves can be observed. A_{peak} values obtained using HVSR are found higher compared to those obtained using GINV. This observation is also reported by many studies done for other regions [Sharma et al. 2013; Field and Jacob, 1995; Ahmadzadeh et al., 2017].

Further, the results of HVSR estimates obtained in the present study are compared with those reported by Chopra et al. [2018] for the same recording stations considered in the present study. Table 1, Column 9 gives the site class as per Di'Alessandro et al. [2012] classification scheme (See Table 3) reported by Chopra et al. [2018]. Consistency between the f_{peak} value for each recording stations (obtained in the present study) and the corresponding site class reported by Chopra et al. [2018] can be observed in Table 1. Further, the comparison of HVSR curves and the average HVSR curves for the corresponding site class (indicated by dashed line) reported by Chopra at al. [2018] shown in Figure11 exhibit 1:1 match in terms of f_{peak} values.

Site	Description
CL-I	f_{peak} < 5 Hz
CL-II	2.5 Hz ≤ f_{peak} ≤ 5 Hz
CL-III	1.66Hz ≤ f_{peak} ≤ 2.5 Hz
CL-IV	f_{peak} > 1.66 Hz
CL-V	f_{peak} not identifiable/flat H/V
CL-VI	Broad amplification/multiple peaks above 5 Hz
CL-VII	f_{peak} not identifiable/multiple peaks over period range

TABLE 3. Site Classification criteria proposed by D'Alessandro et al. (2012).

7. CONCLUSION

In the present study, 156 EQ records from regions in and around the north-west Himalaya are processed and analysed for separating source and site spectra using GINV method. Obtained source spectra is fitted to the theoretical source model to get and. Furthermore, , and are also calculated for the above events. Based on these findings, correlations between the estimated source parameters are proposed leading to the following conclusions;

1) Within the range 4.96 × 10^{13}Nm < M_0 < 2.91 × 10^{16}Nm, M_0 is approximately proportional to f_c^{-3}, with $M_0 f_c^3$=(1.8 × 10^{16}Nm/s3), corresponding to a constant Δσ of 3.5MPa, indicating self-similarity nature of EQs in the region.
2) Value of Δσ for individual EQs varies from 0.53MPa to 21.13MPa with an average of 0.81MPa and the relation between Δσ and σ_A is consistant with the theoretically expected relation of $\sigma_A = 0.23\ \Delta\sigma$ given by Kikuchi and Fukao, [1988] based on global records.
3) Δσ shows no dependence with M, H and M_0.
4) Least square regression between E_S and M_0 yields; $\log E_S = 1.2 \log M_0 - 6$ for in the range of 4.96 × 10^{13}Nm < E_S < 2.90 × 10^{16}Nm.

In addition, STF curves developed based on the results of GINV for horizontal and vertical components shows clear and distinct peak for majority of the recording stations. Values of f_{peak} and A_{peak} obtained from the STF curves are in the range of 0.7 to 6Hz and 2 to 6.9 respectively. STF curves from GINV method is compared with HVSR estimates. Comparison between the two methods shows similarities in terms of the general shape and values of f_{peak}.

Acknowledgements. Authors are thankful for the PESMOS, Department of Earthquake Engineering for providing ground motion records used in the present work. In absence of recorded ground motion, carrying out present work would be impossible.

REFERENCES

Ahmadzadeh, S., S. Parolai, G. Javan-Doloei, and A. Oth (2017). Attenuation characteristics, source parameters and site effects from inversion of S waves of the March 31, 2006 Silakhor aftershocks, Ann. of Geophys., 60(6), 668.

Aki, K. (1967). Scaling law of seismic spectrum, J. Geophys. Res., 72(4), 1217–1231.

Ambraseys, N. N. and J. Douglas (2004). Magnitude calibration of North Indian earthquakes, Geophys. J. Int., 159, 165–206.

Andrews, D. J. (1986). Objective determination of source parameters and similarity of earthquakes of different size, Earthquake source mechanics, 259–267.

Avouac, J. P., F. Ayoub, S. Leprince, O. Konca, and D. V. Helmberger (2006). The 2005, Mw 7.6 Kashmir earthquake: Sub-pixel correlation of ASTER images and seismic waveforms analysis, Earth Planet. Sci. Lett., 249(3), 514–528.

Aydan, Ö., Y. Ohta and M. Hamada (2009). Geotechnical evaluation of slope and ground failures during the 8 October 2005 Muzaffarabad earthquake, Pakistan. J. of Seism., 13(3), 399–413.

Bhattacharya, S.N., J. R Kayal (2005). Seismicity of the Himachal Himalaya: constraint from local seismic network, Geo Survey Ind. Special Publication 85, 71–79.

Bindi, D., F. Pacor, L. Luzi, M. Massa, and G. Ameri (2009). The Mw 6.3, 2009 L'Aquila earthquake: source, path and site effects from spectral analysis of strong motion data, Geophys. J. Int., 179(3), 1573–1579.

Boatwright, J., J.B. Fletcher, and T.E. Fumal (1991). A general inversion scheme for source, site, and propagation characteristics using multiply recorded sets of moderate-sized earthquakes, Bull. Seism. Soc. Am., 81(5), 1754–1782.

Borcherdt, R. D. (1970). Effects of local geology on ground motion near San Francisco Bay, Bull. Seism. Soc. Am., 60, 29–61.

Brune, J. N. (1970). Tectonic stress and the spectra of seismic shear waves from earthquakes, Journal of geophys. Res., 75(26), 4997–5009.

Burrard, S. G. (1910b), Memorandum of the steps taken in 1905-10 to enable movements of the Earth's crust to be detected, in Account of the Operations of the Great Trigonometrical Survey of India, vol. XIX, Descriptions of Heights of Bench Marks of the Northern Lines of Leveling, edited by S. G. Burrad, Surv. of India, Dehra Dun

Burrard, S. G. (1910a), Account of the Operations of the Great Trigonometrical Survey of India, vol. XIX, Descriptions of Heights of Bench Marks of the Northern Lines of Leveling, Surv. of India, Dehra Dun.

Cantore, L., A. Oth, S. Parolai, and D. Bindi (2011). Attenuation, source parameters and site effects in the Irpinia-Basilicata region (southern Apennines, Italy), J. of Seism., 15(2), 375–389.

Castro, R. R., J. G. Anderson, and S. K. Singh (1990). Site response, attenuation and source spectra of S waves along the Guerrero, Mexico, subduction zone, Bull. Seism. Soc. Am., 80(6A), 1481–1503.

Chopra, S., Kumar, V., Choudhury, P., and R. B. S. Yadav (2018). Site classification of Indian strong motion network using response spectra ratios. J. of Seismol., 22(2), 419–438.

Gansser, A. (1964). Geology of the Himalaya, Interscience, New York, 289.

Harbindu, A., S. Gupta and M. L. Sharma, (2014). Earthquake ground motion predictive equations for Garhwal Himalaya, India. Soil Dyn. Earthq. Eng., 66, 135–148.

Harinarayan, N. H. and A. Kumar (2018a). Determination of NEHRP Site Class of Seismic Recording Stations in the Northwest Himalayas and Its Adjoining Area Using HVSR Method, Pure Appl. Geophys., 175(1), 89–107.

Harinarayan, N. H. and A. Kumar (2018b). Seismic Site Classification of Recording Stations in Tarai Region of Uttarakhand, from Multiple Approaches, Geot. Geol. Eng., 1–16.

Harinarayan, N. H. and A. Kumar (2019). Estimation of path attenuation and site characteristics in the north-west Himalaya and its adjoining area using generalized inversion method, Nat. Hazard.

Hassani, B., H. Zafarani, J. Farjoodi, and A. Ansari (2011). Estimation of site amplification, attenuation and source spectra of S-waves in the East-Central Iran, Soil Dyn. Earthq. Eng., 31(10), 1397–1413.

Kayal, J. R. (2001). Microearthquake activity in some parts of the Himalaya and the tectonic model, Tectonophysics, 339(3-4), 331–351.

Kikuchi, M. and Y. Fukao (1988). Seismic wave energy inferred from long-period body wave inversion, Bull. Seism. Soc. Am., 78(5), 1707–1724.

Konno, K. and Ohmachi, T. (1998). Ground-motion characteristics estimated from spectral ratio between horizontal and vertical components of microtremor, Bull. Seism. Soc. Am., 88(1), 228–241.

Kumar, A., H. Mittal, R. Sachdeva and A. Kumar (2012). Indian strong motion instrumentation network, Seismol. Res. Lett., 83(1), 59–66.

Kumar, D., V. Sriram, I. Sarkar, and S. S. Teotia (2008). An estimate of a scaling law of seismic spectrum for earthquakes in Himalaya, Indian Miner. 61(3-4) and 62 (1-4), 83–92.

Kumar, N., J. Sharma, B. R. Arora, and S. Mukhopadhyay (2009). Seismotectonic model of the Kangra-

Chamba sector of northwest Himalaya: Constraints from joint hypocenter determination and focal mechanism, Bull. Seism. Soc. Am., 99(1), 95–109.

Kumar, S., and A. K. Mahajan (1994). The Uttarkashi earthquake of 20 October 1991: field observations, Terra Nova, 6(1), 95–99.

Kumar, V., D. Kumar and S. Chopra (2016). Estimation of source parameters and scaling relations for moderate size earthquakes in North–West Himalaya, J. Asian Earth Sci., 128, 79–89.

Mahajan AK, N. Kumar, B.R Arora (2006). Quick look isoseismal map of 8 October 2005 Kashmir earthquake. Curr. Sci., 91: 356–361.

Malik, J. N. and T. Nakata (2003). Active faults and related Late Quaternary deformation along the northwestern Himalayan Frontal Zone, India, Ann. of Geophys., 46 (5), 917–936.

Mandal, P. and U. Dutta (2011). Estimation of earthquake source parameters in the Kachchh seismic zone, Gujarat, India, from strong–motion network data using a generalized inversion technique, Bull. Seism. Soc. Am., 101(4), 1719–1731.

Menke, W. (2018). Geophysical data analysis: Discrete inverse theory. Academic press.

Mittal, H., A. Kumar, Y. M. Wu and A. Kumar (2016a). Source study of M w 5.4 April 4, 2011 India–Nepal border earthquake and scenario events in the Kumaon–Garhwal Region, Arab. J. Geosci., 9(5), 348.

Mittal, H., Y. M. Wu, D. Y. Chen and W. A. Chao (2016b). Stochastic finite modeling of ground motion for March 5, 2012, Mw 4.6 earthquake and scenario greater magnitude earthquake in the proximity of Delhi, Nat. Hazard., 82(2), 1123–1146.

Mukhopadhyay, S., and J. R. Kayal (2003). Seismic tomography structure of the 1999 Chamoli earthquake source area in the Garhwal Himalaya, Bull. Seismol. Soc. Am., 93(4), 1854–1861.

Mundepi A. K., J. J. Galiana–Merino and C. Lindholm (2010). Soil characteristics and site effect assessment in the city of Delhi (India) using H / V and f–k methods, Soil Dyn. Earthq. Eng., 81, 767–773.

Oth, A. and A. E. Kaiser (2014). Stress release and source scaling of the 2010–2011 Canterbury, New Zealand earthquake sequence from spectral inversion of ground motion data, Pure Appl. Geophys., 171(10), 2767–2782.

Oth, A., D. Bindi, S. Parolai, and F. Wenzel (2008). S–wave attenuation characteristics beneath the Vrancea region in Romania: new insights from the inversion of ground–motion spectra, Bull. Seism. Soc. Am., 98(5), 2482–2497.

Philip, G., N. Suresh and S. S. Bhakuni (2014). Active tectonics in the northwestern outer Himalaya: evidence of large–magnitude palaeoearthquakes in Pinjaur Dun and the Frontal Himalaya, Curr. Sci., 106, 211–222.

Sarkar, I., Pachauri, A. K. and M. Israil (2001). On the damage caused by the Chamoli earthquake of 29 March, 1999, J. Asian Earth Sci., 19: 129–134.

Sharma, J., S. Chopra and K. S. Roy (2013). Estimation of source parameters, quality factor (QS), and site characteristics using accelerograms: Uttarakhand Himalaya region, Bull. Seism. Soc. Am., 104(1), 360–380

Valdiya, K. S. (1984). Evolution of the Himalaya, Tectonophysics, 105(1–4), 229–248.

Vassiliou, M. S. and H. Kanamori (1982). The energy release in earthquakes, Bull. Seism. Soc. Am., 72(2), 371–387.

Wallace, K., R. Bilham, F. Blume, V. K. Gaur and V. Gahalaut (2005). Surface deformation in the region of the 1905 Kangra Mw= 7.8 earthquake in the period 1846–2001, Geophys. Res. Lett., 32(15), doi: 10.1029/2005GL022906.

Zafarani, H., Hassani, B. and A. Ansari (2012). Estimation of earthquake parameters in the Alborz seismic zone, Iran using generalized inversion method, Soil Dyn. Earthq. Eng., 42, 197–218.

*CORRESPONDING AUTHOR: Kumar ABHISHEK,
Department of Civil Engineering,
Indian Institute of Technology Guwahati, Assam, India;
email: abhitoaashu@gmail.com/ abhiak@iitg.ernet.in